Dalton Transactions

On the Use of NMR Distance Measurements for Assessing Surface Site Homogeneity

Journal:	*Dalton Transactions*
Manuscript ID	DT-ART-09-2023-003201.R1
Article Type:	Paper
Date Submitted by the Author:	15-Nov-2023
Complete List of Authors:	Perras, Frédéric A.; Ames Laboratory, Chemical and Biological Sciences Culver, Damien; Ames Laboratory,

ARTICLE

On the Use of NMR Distance Measurements for Assessing Surface Site Homogeneity

Frédéric A. Perras*[a,b] and Damien B. Culver[a]

Received 00th January 20xx,
Accepted 00th January 20xx

DOI: 10.1039/x0xx00000x

The past decades have seen tremendous growth in the area of single-site heterogeneous catalysis which aims to marry the best aspects of homogeneous and heterogeneous catalysis, namely molecular-level site control and ease of separation/recycling. Despite this, we still do not have a means of assessing site homogeneity and whether the produced catalyst is indeed "single-site". Recent developments have enabled the use of NMR-based distance measurements to determine the conformations and configurations of surface sites, leading to the question whether such measurements can be used to distinguish materials containing either single or multiple surface sites with otherwise indistinguishable NMR properties. We describe a Monte Carlo-based multi-structure search algorithm and its application to the determination of multi-site structures from supported metal complexes. The sensitivity of REDOR data to the existence of multiple sites is assessed using synthetic data and prior literature examples are revisited to determine whether the single-site approximation was indeed appropriate. We lastly apply this new methodology to differentiate the configurations of zirconocene complexes grafted onto alumina supports that were thermally treated at different temperatures.

Introduction

Dynamic nuclear polarization (DNP) surface-enhanced nuclear magnetic resonance (NMR) spectroscopy (DNP SENS)[1-3] has led to a dramatic rise in the applications of NMR to the study of heterogeneous catalysts.[4-6] Among the new possibilities that have been made available by the technique has been the high-resolution structural characterization of surface sites using NMR-based distance measurements. This idea was initially introduced by Berruyer *et al.* in 2017 who used site-labeled complexes to perform atom-to-atom distance measurements and use these for distance constraints in a brute-force distance geometry conformational search.[7] We later expanded on this concept by applying surface-to-atom distance measurements, which can be modeled accurately using multispin simulations.[8,9] This later strategy has been applied to a growing number of supported metal complexes, and has made use of surface ^{17}O, ^{27}Al, ^{29}Si, ^{133}Cs, and ^{207}Pb nuclei.[8-14]

Recently, Jabbour *et al*. have applied the strategy introduced by Berruyer *et al*. to study the surface structure of an Ir NHC complex.[11] Using a ^{13}C-labelled NHC they could detect not only the simultaneous presence of free and coordinated ligand, but a ^{13}C-^{13}C correlation experiment also showed the existence of surface Ir centers coordinated to two NHC ligands. A similar observation was later made on an analogous Pt complex.[15] The revelation that this simple complex contained as many as three distinct surface NHC species has important implications to the manner in which surface structure determinations have been performed.

The distance geometry strategy introduced by Berruyer *et al*.[7] makes a key assumption that the structure can be described by a single site. This assumption originates from the approach's roots in biomolecular NMR structure determinations of proteins, which tend to adopt a single conformation.[16] In sites supported on amorphous surfaces, however, this assumption is difficult to justify.[11,15,17] We thus sought to determine whether solid-state NMR-based distance measurements could be used to resolve distinct conformers with overlapping resonances. Indications that this may be possible originate from the concept of inverting rotational-echo double-resonance (REDOR)[18] data and "de-Pake-ing".[19-22] Analogous regularization approaches are commonly used to extract overlapping distances from a single double electron-electron resonance (DEER) dataset.[23-25] Herein, we describe a Monte Carlo-based multi-structure distance geometry algorithm for the solution of surface structures using REDOR data. The performance of the method is evaluated using synthetic data calculated for known compounds. We then reevaluate experimental data acquired from these compounds in an attempt to determine whether the existing 1-site fitting strategy is indeed justified or whether the compounds in question contain multiple surface sites.

Finally, we deliberately synthesize an Al_2O_3-supported Zr complex expected to contain multiple sites and attempt to distinguish these using DNP-enhanced NMR-based distance measurements and the aforementioned algorithm.

Experimental

[a] *Chemical and Biological Sciences Division, Ames National Laboratory, Ames, IA 50011, USA.*
[b] *Department of Chemistry, Iowa State University, Ames, IA 50011, USA.*
*fperras@ameslab.gov
Electronic Supplementary Information (ESI) available: Supplementary REDOR simulations, data tables, and synthesis and characterization details. See DOI: 10.1039/x0xx00000x

Solid-State NMR

All solid-state NMR experiments were carried out using a 400 MHz/264 GHz Bruker MAS-DNP spectrometer equipped with an AVANCE III console, and a 3.2 mm probe. The probe was tuned in a double-resonance configuration and a REDOR box was used to split the channel into two, such that ^{1}H-^{13}C-^{27}Al triple-resonance experiments could be performed.[26] Samples were impregnated with a 16 mM solution of TEKPol[27] in dry perdeuterated 1,1,2,2-tetrachloroethane (TCE-d2),[28,29] packed into sapphire rotors in an Ar glovebox, and spun to an MAS rate of 10 kHz. Hyperpolarized ^{1}H magnetization was excited using a 2.5 µs 90° pulse and transferred to ^{13}C using 1 ms of cross-polarization (CP). ^{13}C-^{27}Al dipolar interactions were reintroduced using REDOR recoupling[18] with 8 µs ^{13}C inversion pulses. A 150 µs, 100 kHz, ^{27}Al saturation pulse was applied to prevent the refocusing of dipolar interactions in the rotational-echo saturation-pulse double-resonance (RESPDOR) experiments.[30] Dipolar recoupling times were incremented in steps of 0.4 ms, with the exception of the 1000 °C sample where this was increased to 0.8 ms, to a final value of 5 ms. Each subspectrum was acquired in 1280, 1280, 640, and 4096 scans for the 400, 600, 800, and 1000 °C samples, respectively, with a 1.5 s recycle delay, corresponding to a time of $1.3T_{DNP}$.

Structure Determination.

All structure determinations were performed using the open-source INTERFACES program,[12] which was recently updated to include the routines described in the theory section. In all cases, the number of conformers considered for the multi-structure fits was set to two.

For the Al_2O_3-supported Ir pincer,[9,31] the structure search consisted of varying the distance between the complex and the surface in 31 steps of 0.1 Å and rotating the complex around the N-Ir-N axis in steps of 5°. 1 million pairs of conformers were tried for the multi-structure search.

The conformation of the SiO_2-tetheted Pt NHC complex[7] was performed by stepping each rotatable bond dihedral in 20° increments, and also varying the TMS-NHC T site distance in four steps of 1 Å. The multi-structure search consisted of an evaluation of 100 million conformer pairs.

The structure of the SiO_2-tethered Zn phenanthroline complex[10] was searched in 100 million steps wherein the dihedral angles of all four rotatable bonds were stepped in 10° increments.

The configuration of the SiO_2-grafted Sc amidinate complex[10,32] was searched in 100 million iterations wherein the N-*i*Pr dihedral angles were stepped in 90° increments, in addition to the Sc-amidinate angles, which enables the evaluation of both trigonal bipyramidal and square pyramidal configurations. The bond angle of the surface tether was also stepped in 10° increments, while the complex was also allowed to rotate in 40° increments around this tether.

The configuration of the Al_2O_3-supported zirconocene complex was determined in 5580 steps wherein the distance between Zr and the surface was searched in 31 steps of 0.1 Å and the orientation of the complex was stepped in 2° increments.

Theory

Simulation of Multi-site REDOR data

The conformations and orientations of supported complexes can be determined using NMR-based distance measurements that make use of the REDOR experiment, or its derivatives (such as RESPDOR and symmetry-based (S)-REDOR).[18,30,33,34] Due to sensitivity limitations, these are often performed using some form of sensitivity enhancement, such as DNP, ^{1}H-detection, and isotope enrichment. These experiments measure the direct dipolar coupling interaction between nuclei, which is characterized by the dipolar coupling constant (D).

$$D = \frac{\mu_0 \hbar \gamma_1 \gamma_2}{4\pi \ 2\pi} \langle r^{-3} \rangle \quad (1)$$

In equation 1, μ_0 represents the permeability of free space, γ_i the gyromagnetic ratios of the coupled nuclei, and $\hbar$ the reduced Planck constant. In a typical REDOR measurement, experiments are performed in pairs, where the application of a pulse on the second, recoupled, channel is either applied or omitted. The latter experiment is used to normalize the dataset with respect to T_2 decay; the intensity of the NMR signal in that experiment is termed S_0. The signal intensity of the dipolar dephased experiment is termed S, and the normalized dephasing is typically presented as a normalized difference: $\Delta S/S_0$. The value of $\Delta S/S_0$ depends on the duration of the recoupling (τ_{rec}), D, and the orientation of the internuclear vector with respect to the rotor axis, as characterized by the polar angles α and β.

$$\frac{\Delta S}{S_0}(\tau_{rec}) = 1 - \frac{f}{4\pi}\int_0^{2\pi}\int_0^{\pi}\cos\left(2\sqrt{2}D\tau_{rec}\sin 2\beta \sin\alpha\right)\sin\beta \, d\alpha \, d\beta \quad (2)$$

In equation 2, f is a factor used to compensate for imperfections that may reduce the overall dephasing level. This approach to predicting REDOR dephasing levels also lends itself to the prediction of REDOR data in multispin systems, such as from the interaction of a single ^{13}C nucleus with a group of ^{29}Si nuclei from a silica surface. In that case, the total dephasing level is simply the product of the dephasing from each spin pair, as REDOR recouples these interactions independently.[35]

$$\frac{\Delta S}{S_0}(\tau_{rec}) = 1 - \frac{f}{8\pi^2}\int_0^{2\pi}\int_0^{\pi}\int_0^{2\pi}\prod_{i=1}^{N}\cos\left(2\sqrt{2}D\langle S\rangle\tau_{rec}\sin 2\beta_i \sin\alpha_i\right)\sin\beta \, d\alpha \, d\beta \, d\gamma. \quad (3)$$

To date, structure determinations using REDOR data have utilized brute force structure search algorithms wherein structural variables including distances, angles, and dihedrals, are sampled to find the structure that best agrees with the experimental REDOR data.[7,12] The quality of the fit is conveniently quantified using a χ^2 metric, that also enables for statistical analysis. For a given dataset, indexed as i, this is calculated as follows.

$$\chi_i^2 = \sum_{\tau_{rec}} \frac{\left(\Delta S/S_{0,i,expt} - \Delta S/S_{0,i,calc}\right)^2}{\left(\Delta S/S_{0,i,expt}\right)^2} \quad (4)$$

For instance, all structures that are acceptable within a given confidence interval (CI) have χ^2 values that are below a threshold calculated as:[12]

$$\chi^2_{i,max} = \left(2\left(\mathrm{erf}^{-1}(CI)\right)^2 + 1\right)\chi^2_{i,min} \quad . \quad (5)$$

where χ^2_{min} is the lowest value found during the structure search.

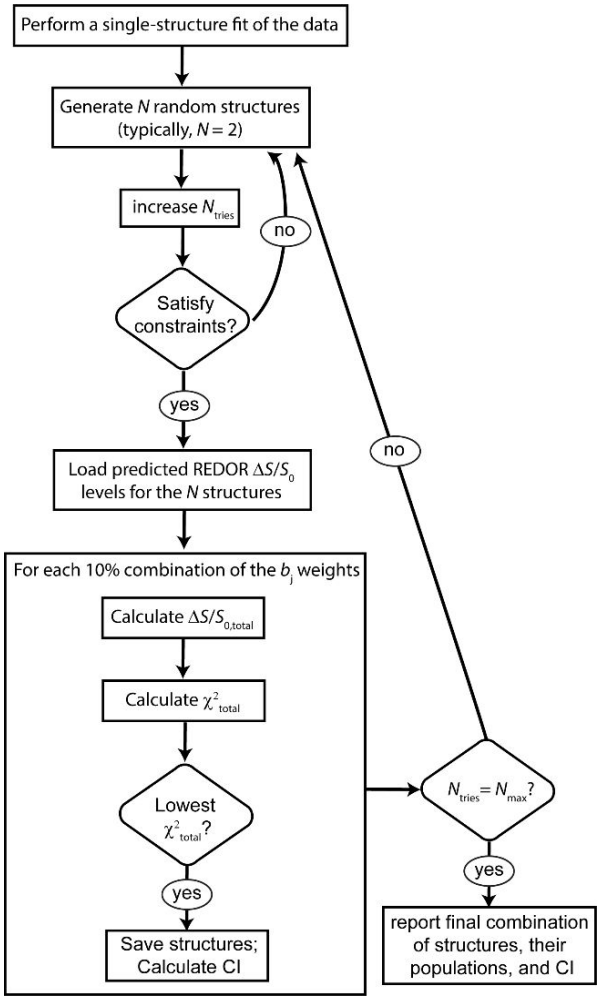

Figure 1. Flowchart describing the process used for the multi-structure REDOR data fitting.

The prediction of REDOR dephasing levels in samples containing mixtures of conformers is easily achieved by a weighted sum of the dephasing levels calculated for the individual conformers. Note that this assumes that all conformers have identical T_2 relaxation times and that this may not be the case in practice.

$$\frac{\Delta S}{S_0}(\tau_{\mathrm{rec}})_{\mathrm{total}} = \sum_{\mathrm{conformers}} b_{\mathrm{j}} \frac{\Delta S}{S_0}(\tau_{\mathrm{rec}})_{\mathrm{j}} \quad (6)$$

In equation 6, the coefficients b_j are the concentrations of the various conformers, indexed as j.

$$\sum_{\mathrm{conformers}} b_{\mathrm{j}} = 1 \quad (7)$$

Structure Search Algorithm

While previous applications of REDOR NMR experiments to the determination of surface structures have applied brute force searches, wherein each dihedral angle is searched in small increments, this approach is intractable for multi-site structure fitting.[7,12] For instance, if we consider a molecule with 6 degrees of rotational freedom, each of which being searched in 10° increments, then there are 36^6=2.18x10^9 conformers to sample. This is easily done using modern computer hardware, but the same elucidation wherein two conformers are fitted independently, together with their relative concentration in 10% increments, requires the evaluation of 11*36^{12}=5.21x10^{19} combinations of conformers. As such, we have opted instead for a Monte Carlo search strategy wherein structural variables are searched at random and the obtained χ^2 for this combination of structures is compared to an extensive single-structure search to determine whether the improvement in agreement with the experimental data is statistically meaningful. The overall process is depicted in **Figure 1**.

Briefly, we start with an exhaustive single structure search and then iterate over a series of N_{max} combinations of N structures that are generated using random values for the structural variables being optimized (distances, angles, dihedrals). We then load precomputed REDOR dephasing data for the N structures, using data libraries, and take linear combinations of these data by stepping b_j values in increments of 10%. The combination of b_j values leading to the lowest χ^2_{total} is then compared to the lowest running χ^2_{total} value and that from the single-structure search to determine if there was an improvement. Any structures that do not pass any constraints specified by the input, or which involve collisions between non-bonded atoms or between an atom and the support, are ignored.

Once N_{max} combinations of structures have been evaluated, the reliability of the multi-structure fit is evaluated using equation 8. Only when there is significant improvement in the quality of the fit will the confidence interval be significant and only then can a multiple-structure fit be deemed significant.

$$CI = \mathrm{erf}\sqrt{\frac{\chi^2_{\mathrm{single}}}{2\chi^2_{\mathrm{i,multi}}} - \frac{1}{2}} \quad (8)$$

Results and Discussion

The following four subsections describe the application of the multisite fitting strategy described in the theory section to four different surface species whose structures have been determined and analyzed elsewhere.[7,9,10] We consider two extremes of their possible conformations and use the INTERFACES program[12] to generate idealized REDOR or RESPDOR data for the two structures. Linear combinations of these datasets are then taken corresponding to mixtures of the two conformers in concentrations ranging from 50 to 100%. We then add a specified level of Gaussian noise to the data and then apply the multisite structure determination approach from the theory section, which is currently available in the INTERFACES GitHub,[36] to see whether the program can indeed recover the two correct structures and their relative populations. Example synthetic data is shown in **Figure S1** at different signal-to noise (S/N) levels. Gaussian noise is added as follows, where rand(1 to -1) indicates the generation of a random number between 1 and -1.

$$\frac{\Delta S}{S_0}(\tau_{\mathrm{rec}}) = \frac{\Delta S}{S_0}(\tau_{\mathrm{rec}})_{\mathrm{ideal}}\left(1 + \frac{N}{S}\sqrt{2}\exp\left(\tau_{\mathrm{rec}}/T_2\right)\mathrm{erf}^{-1}(\mathrm{rand}(1\ \mathrm{to}-1))\right) \quad (9)$$

This function generates noise of an amplitude that increases with τ_{rec} according to a T_2 relaxation decay. The specified signal-to-noise ratio then corresponds to its value when τ_{rec}=0, and increases with the recoupling time, as is typical of real experimental data. In all cases, the T_2 value was set to the

maximum τ_{rec} value used. No synthetic noise was added to experimental data.

Al_2O_3-Supported Ir Pincer

In 2021, we reported the application of surface-to-atom $^{13}C\{^{27}Al\}$ RESPDOR to determine the configuration of an Al_2O_3-supported (^{dm}Phebox)Ir(OAc)$_2$(OH$_2$) complex.[9] The complex could graft in either monopodal or bipodal arrangements, corresponding to the Ir center forming either one or two bonds with surface aluminols. The main conclusion obtained from the RESPDOR data itself was that it was inconsistent with a monopodal structure, which would lead to the formation of a more prone complex and homogeneous ^{13}C-Al_2O_3 distances. It is nevertheless of interest to determine whether there might have been a distribution of both monopodal and bipodal sites on the surface, with the latter being more abundant.

Example surface orientations consistent with mono and bipodal sites are shown in **Figure 2**, and their idealized $^{13}C\{^{27}Al\}$ RESPDOR simulations are shown in **Figure S2**. Data corresponding to mixtures of the two configurations with six bipodal concentrations ranging from 100% to 50% were then synthesized and a multi-site structure solution was performed at various noise levels. Each structure solution was then repeated 5 times for each noise level. The averaged results from these searches are summarized in **Figure 2c-e** and the raw data are tabulated in **Tables S1-S6**.

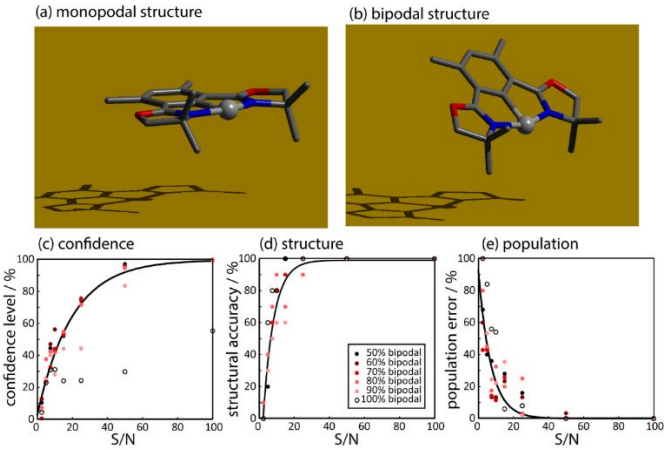

Figure 2. Three-dimensional representation of the monopodal (a) and bipodal (b) (^{dm}Phebox)Ir/Al_2O_3 structural models used to generate synthetic $^{13}C\{^{27}Al\}$ RESPDOR datasets. Plots of the S/N-dependence of the confidence level for the multi-structure fits (c), the accuracy of the determined structures (d), and the relative populations of the determined structures (e) are shown on the bottom. Results are shown for synthetic mixtures of the two components in 50-100% concentration for the monopodal constituent.

We can see in **Figure 2c** that, as expected, the confidence interval of the multi-site fit (equation 8) increases with increasing S/N in an exponential manner. All concentrations follow the same line, with the exception of the 100% bipodal model that maintains a very low confidence that there are two sites, as would be expected.

In a similar, albeit steeper, trend, we can see that the percentage of the determined structures that are qualitatively correct increases with increasing S/N (**Figure 2d**). Interestingly, this suggests that the confidence interval metric underestimates the reliability of the structures and that accurate structures are expected at S/N values above 20.

The accuracy of the population of the two sites also increases with increasing S/N (**Figure 2e**) and in this, and other (*vide infra*), samples is found to correlate relatively well with the confidence interval (**Figure S6**). It would thus seem that the confidence interval can be used directly to estimate the uncertainty in the determined site populations ($\sigma_{population}$, equation 10). A factor of ½ in equation 10 is included to reflect the fact that the error in the relative site populations equals $2\sigma_{population}$.

$$\sigma_{population} = \frac{100\% - CI}{2} \quad (10)$$

It would thus seem from this analysis that prior experimental $^{13}C\{^{27}Al\}$ RESPDOR data should be sufficient to distinguish mixtures of mono and bipodal sites given that the signal to noise ratio surpasses ~30. This data from reference 9 is reproduced in **Figure 3**.

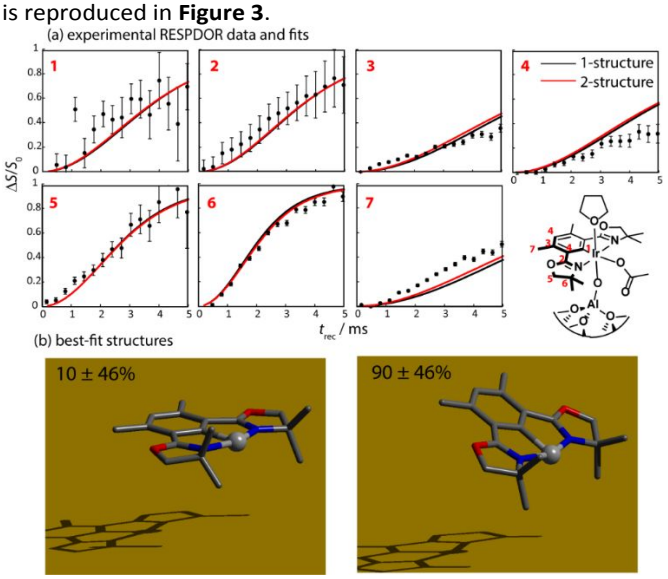

Figure 3. (a) Experimental $^{13}C\{^{27}Al\}$ RESPDOR data obtained for (^{dm}Phebox)Ir/Al_2O_3.[9] Fits are shown that include only a single molecular model (black) or two (red). The best-fit structures from the 2-structure fit are shown in (b) together with their fitted concentrations.

Performing a single-structure fit on this data yielded the fits shown in black in **Figure 3** and a structure that agreed with that from the prior study. A multisite structure determination was then performed, which only managed to reduce the χ^2 from 9.62 to 9.51, corresponding to a confidence interval of 8.7%. This best-fit 2-structure combination was composed of 90% bipodal and 10% monopodal sites, however, the uncertainties in these populations equal 46% which indicates that we cannot conclude the existence of a second site. When considering that our analysis of synthetic data revealed that we should be able to differentiate multiple sites in this compound, we can thus conclude that the supported complexes in this material are homogeneous in their podality and form overwhelmingly bipodal species.

SiO_2-Tetheted Pt NHC

We next revisit the tethered Pt N-heterocyclic carbene (NHC) complex, initially studied by Berruyer *et al.* in 2016.[7] In their study, they used ^{13}C,$^{29}Si\{^{15}N\}$ REDOR data on two singly ^{15}N-labelled analogues of the complex to obtain a series of distance constraints for a 3D structure determination. They concluded, based on the observation of a shifted TMS ^{29}Si signal, and its interactions with the aforementioned ^{15}N spins, that the Pt formed a secondary interaction with the siloxane of this moiety. The analysis, however, assumes site homogeneity and that all Pt centers have this intermolecular interaction between Pt and the TMS groups. This may not necessarily be the case.

As was done for the Ir pincer complex, we designed two extreme conformers that either include or exclude this interaction (**Figure 4a,b**). The predicted REDOR data are given in **Figure S3**, which show notable differences suggesting that we may be able to differentiate the two conformers using REDOR. Taking a 50:50 mixture of these two sites, we again evaluated the reliability of a multisite fit on this system, the results of which are shown in **Figure 4c-e** and **Table S7**. We broadly observe the same dependence as was seen for the Ir complex, suggesting that with S/N values above ~30 that we can reliably differentiate these two sites in a mixture.

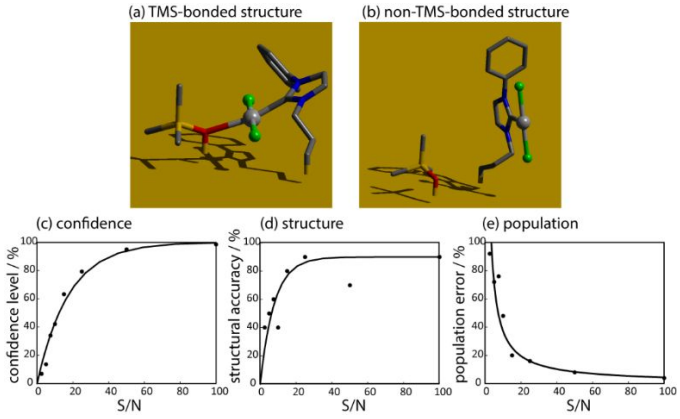

Figure 4. Three-dimensional representation of the TMS-bonded (a) and non-TMS-bonded (b) (NHC)Pt/SiO_2 structural models used to generate synthetic ^{13}C,$^{29}Si\{^{15}N\}$ REDOR datasets. Plots of the S/N-dependence of the confidence level for the multi-structure fits (c), the accuracy of the determined structures (d), and the relative populations of the determined structures (e) are shown on the bottom, all calculated for a 50:50 mixture of the structures in (a) and (b).

A new analysis of the experimental data from reference 7 was performed to search for potential minor species (**Figure 5**). The result was a more sizeable reduction in χ^2 from 9.04 to 6.86, corresponding to a confidence of 43% that there are multiple sites. The major structure, corresponding to an estimated 80% of the surface sites, was indeed that determined by Berruyer *et al,* with a minor unbound species. This secondary species' low population of 20 ± 29%, nevertheless indicates that we cannot conclude its existence outside error. The results are thus consistent with the earlier analysis that there is a dominant species interacting with surface TMS groups, with no minor species being identifiable outside of error.

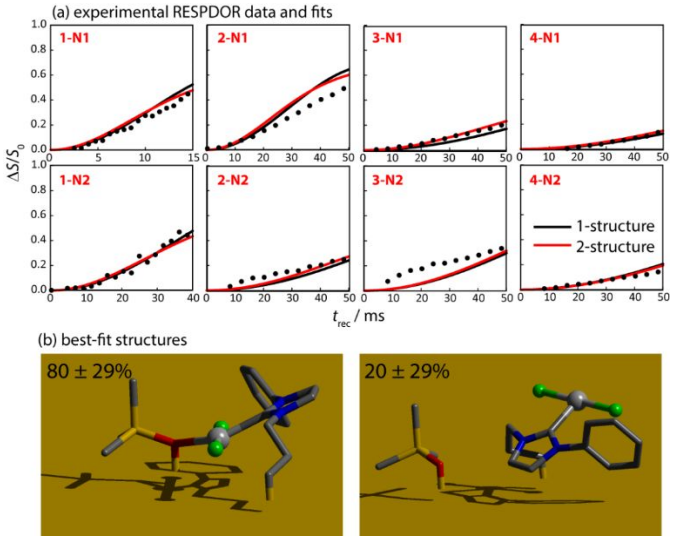

Figure 5. (a) Experimental ^{13}C,$^{29}Si\{^{15}N\}$ REDOR data obtained for (NHC)Pt/SiO_2. Fits are shown that include only a single molecular model (black) or two (red). The best-fit structures from the 2-structure fit are shown in (b) together with their fitted concentrations.

In this particular type of application, wherein the bulk of the structural constraints come from intermolecular contacts, it is important to consider potential issues caused by there being an excess of a particular site. For instance, if there were insufficient TMS groups to bind with each Pt site, we would nevertheless determine the same structure while there could be "invisible" Pt centers that do not possess such an interaction. In fact, a later study found that this system did indeed contain multiple sites.[15]

SiO_2-Tethered Zn Phenanthroline

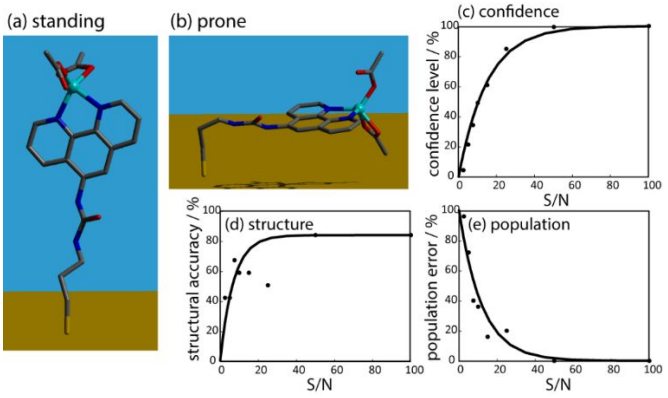

Figure 6. Three-dimensional representation of the standing (a) and prone (b) Zn/Phen-SiO_2 structural models used to generate synthetic $^{13}C\{^{29}Si\}$ REDOR datasets. Plots of the S/N-dependence of the confidence level for the multi-structure fits (c), the accuracy of the determined structures (d), and the relative populations of the determined structures (e) are shown on the right, all calculated for a 50:50 mixture of the structures in (a) and (b).

In 2021 we used $^{13}C\{^{29}Si\}$ REDOR experiments to probe the proximity between carbon sites in various complexes and the silica surface to determine their conformations.[10] Among these, was a tethered Zn phenanthroline complex which was found to form potential secondary Zn-silica interactions, as evidenced by

its prone conformation being more proximate with the silica than in the free ligand. We thus sought to determine, using the approach described herein, whether mixtures of prone and upright complexes (**Figure 6a,b**) are indeed distinguishable.

As we did in the case of the Pt complex, we generated a synthetic 50:50 mixture of these two species to probe the possibility of the task *in silico.* The synthetic data calculated for each conformer are shown in **Figure S4** with the final results shown in **Figure 6c-e** and tabulated in **Table S8**. The drastic difference between the species means that they are easily differentiated, however we found that the accuracy of the upright conformation was reduced due to the weak ^{13}C -^{29}Si interactions in this orientation. The reliability with which the program could discern the existence of a second site, and its abundance, was, however, quite reasonable.

The experimental data from reference 10 is reproduced in **Figure 7** where we again show the results from fits obtained with 1 and 2 conformers. The χ^2 could be reduced from 15.9 to 14.2, corresponding to a negligible confidence that there are two sites of 27%. The major species corresponded to the previously determined conformer at a 70% concentration while the secondary structure was also in a prone conformation, albeit rotated relative to the main structure. The existence of a second site could not be affirmed outside of error and the determined fit suggests that such a second site would be very similar to the primary one. We can again, thus, reasonably conclude that there is primarily a single species in this material.

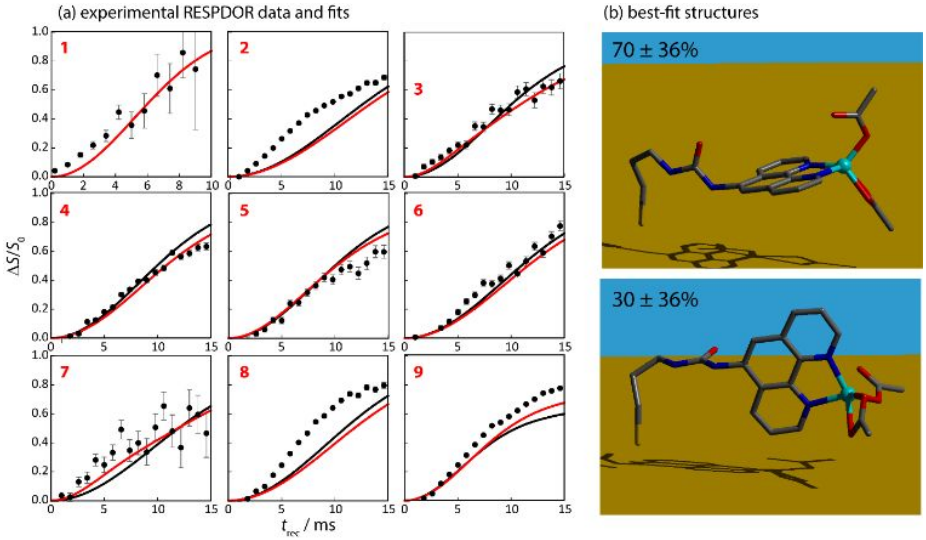

Figure 7. (a) Experimental $^{13}C\{^{29}Si\}$ REDOR data obtained for Zn/Phen-SiO_2. Fits are shown that include only a single molecular model (black) or two (red). The best-fit structures from the 2-structure fit are shown in (b) together with their fitted concentrations.

SiO_2-Grafted Sc Amidinate

The last complex we are revisiting from prior literature is a Sc amidinate complex that is grafted to ^{29}Si-enriched silica. Similarly, to the Zn sample, this complex's conformation was studied using surface-to-atom $^{13}C\{^{29}Si\}$ REDOR experiments.[10] The main structural unknown for this complex is its coordination geometry which could exist as trigonal bipyramidal or square pyramidal. We thus took the previously determined conformation and rotated one amidinate ligand by 90° to produce a trigonal bipyramidal structure that is as close to the square pyramidal structure as possible (**Figure 8a,b**).

The predicted REDOR data for these two configurations are shown in **Figure S5** and are in fact quite similar. This similarity is also reflected in the results obtained when attempting to differentiate them in a synthetic 50:50 mixture (**Figure 8c-e**, **Table S9**). We found that even with a S/N of 100 that the software could only correctly identify one of the two structures (the square pyramidal one). This compound has the most degrees of freedom of the compounds in this paper and is difficult to sample in a Monte Carlo manner. Probabilistically, more square pyramidal conformers avoid contacting the surface and thus more of them are considered in the multisite fitting.

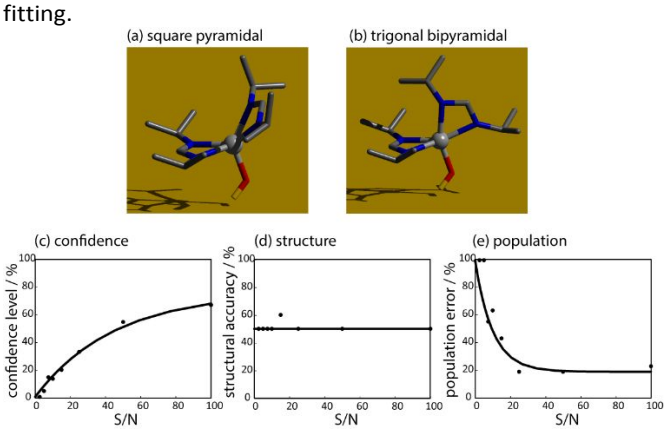

Figure 8. Three-dimensional representation of the square pyramidal (a) and trigonal bipyramidal (b) $(\kappa^2\text{-}(N\textit{i}Pr)_2CH)_2Sc/SiO_2$ structural models used to generate synthetic $^{13}C\{^{29}Si\}$ REDOR datasets. Plots of the S/N-dependence of the confidence level for the multi-structure fits (c), the accuracy of the determined structures (d), and the relative populations of the determined

structures (e) are shown on the bottom, all calculated for a 50:50 mixture of the structures in (a) and (b).

When we fit the experimental data to a 2-site model, the χ^2 was reduced from 0.78 to 0.58, corresponding to a 43.7% confidence interval (**Figure 9**). Again, this is quite low, but considering the confidence intervals calculated in the idealized model (**Figure 8c**), this may be significant. As expected, both sites were determined to be square pyramidal, but their site populations of 60 ±28 and 40 ± 28 % suggest that there are likely multiple sites in this material. This is consistent with a previous study that found the ^{45}Sc quadrupolar coupling parameters to be distributed, something that was reproduced by density functional theory (DFT) calculations of sites grafted to different silanols on amorphous silica.[32] While we cannot expect to reliably elucidate the configurations of the Sc sites, the data suggests that we can conclude that this material is in fact heterogeneous and contains an array of different conformations or configurations.

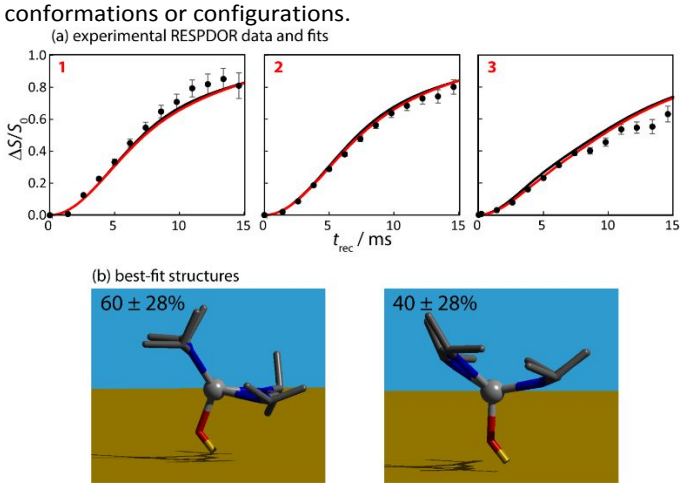

Figure 9. (a) Experimental $^{13}C\{^{29}Si\}$ REDOR data obtained for $(\kappa^2\text{-}(N\textit{i}Pr)_2CH)_2Sc/SiO_2$. Fits are shown that include only a single molecular model (black) or two (red). The best-fit structures from the 2-structure fit are shown in (b) together with their fitted concentrations.

Al_2O_3-Grafted Zirconocene

The assessments performed on the literature examples that were discussed in the preceding subsections showed that under favorable circumstances it should be possible to identify multiple surface species outside of error using only REDOR data. Most of the examples shown to date, however, do not show significant evidence for the existence of multiple sites. To determine whether such structure determinations are indeed possible, we supported a zirconocene complex ($Me_2SiCp_2ZrMe_2$) on the surface of γ-Al_2O_3 activated at temperatures of 400, 600, 800, and 1000 °C (see SI for details). As with complexes grafted to silica surfaces, we expect that grafting can lead to the formation of bi or monopodal species through protonolysis reactions with surface aluminols (**Figure 10a,b**), but the complex can also react with the Lewis acid sites that are present on the surface and form a cationic species through methyl abstraction (**Figure 10c**).[9] Increases in activation temperature should reduce the concentration of surface hydroxyls and disfavor the formation of bipodal species. Further increases in temperature are also expected to lead to a larger number of Lewis acid sites as the surface becomes drier.[37] The lowest temperature we selected, 400 °C, is lower than the 450 °C used in the synthesis of the bipodal Ir complex described earlier[9] and should produce an alumina surface with roughly 5 OH nm^{-2},[38,39] which is higher than that found in non-thermally treated silica.[40] As such, this temperature maximizes the chances of producing a bipodal species.

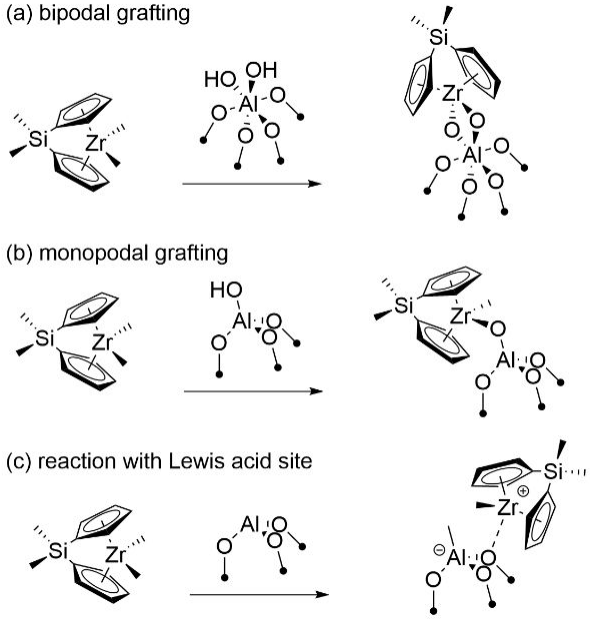

Figure 10. Possible grafting reactions between a zirconocene complex and thermally activated γ-Al_2O_3. Grafting can either proceed through protonolysis and the formation of bi or monopodal species (a and b, respectively) or through methyl abstraction at a Lewis acid site (c).

Measuring the average number of methane molecules that are released for every chemisorbed Zr atom should provide some insight into the monopodal, bipodal, and cationic site content. Mass balances of the chemisorption reactions indicate that 1.6, 1.2, 0.8, and 0.6 equivalents of methane are released per surface bound zirconium for γ-Al_2O_3 activated at 400, 600, 800, and 1000 °C, respectively (see SI for details). This result indicates that each material indeed contains multiple sites. CH_4:Zr ratios >1, as seen in the 400 and 600 °C samples, imply the existence of bipodal and other sites and ratios <1, seen in the 800 and 1000 °C samples, similarly indicating the presence of cationic sites along with protonolysis products.

Spectroscopically, we should be able to distinguish between bipodal and monopodal/cationic species by the fact that they would differ in their orientation with respect to the support surface, as previously demonstrated on the Ir complex revisited. Specifically, due to the tetrahedral geometry of Zr, we would expect bipodal complexes to form a ~90° angle between the Zr-Si vector and the surface plane while this angle would be closer to 0° in the monopodal and cationic complexes.

In all four samples we observed a broad signal from 125 to 105 ppm, due to the overlap of the three chemically inequivalent ^{13}C sites in the Cp moieties, a broad signal at 25 ppm from Zr-CH_3 groups, and a sharper resonance at -5 ppm from the two Si-CH_3 groups.[41] The relative intensity of the Zr-CH_3 signal was comparable in all four samples, suggesting a high level of monopodal Zr throughout the series (**Figure S7**).

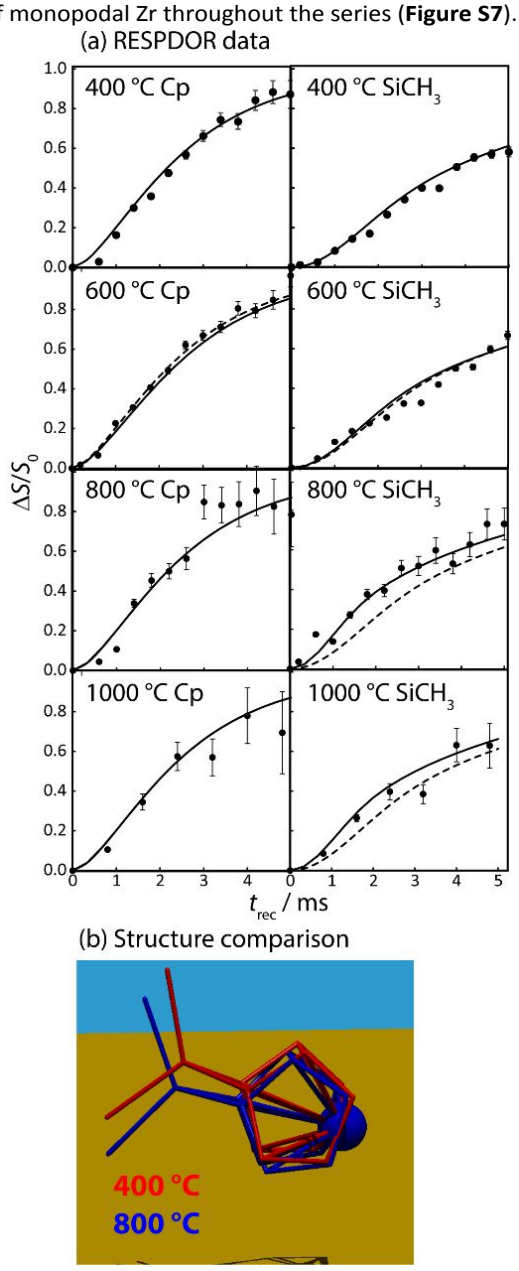

Figure 11. (a) Comparison of the $^{13}C\{^{27}Al\}$ RESPDOR data acquired on the Zr/Al_2O_3 complex grafted on alumina thermally treated at different temperatures, as indicated on the Figure. Dashed lines represent the best-fit curves from the 400 °C sample. (b) Overlay of the best-fit molecular orientations determined for the 400 and 800 °C samples.

The $^{13}C\{^{27}Al\}$ RESPDOR data acquired on the four Zr/Al_2O_3 complexes are shown in **Figure 11**. Due to resolution and T_2 limitations, we could only extract two RESPDOR datasets corresponding to the Si-CH_3 groups, and the Cp carbon sites in aggregate. This is nevertheless sufficient information to allow us to gauge relative complex orientations. Notably, while comparable dephasing rates were measured for the Cp sites in all four materials, the 800 and 1000 °C samples showed a significantly faster dephasing for the Si-CH_3 groups, suggesting that they are situated closer to the surface, as would be expected from a monopodal complex as compared to a bipodal one. This difference is highlighted in **Figure 11** where the best-fit curves from the 400 °C sample are shown as dashed lines in the other datasets.

Despite the visual cues that the materials contain variable levels of bi and monopodal sites, we were able to obtain nearly perfect agreement with the data using structural models that incorporate only a single configuration. Instead, we see that the surface-Zr-Si angle in the best-fit single-structure search gradually decreases from 24 to 21, 14, and finally 16° as the pre-treatment temperature is increased from 400 to 600, 800, and 1000 °C. The variation in this angle is undoubtedly caused by variations in the mono and bipodal site concentrations with the fit merely reporting on a weighted average structure. The gradual decline of the angle as the temperature is increased implies an increase in the concentration of monopodal sites, which agrees with the mass balance data. The relatively low angle of 24° measured in the 400 °C sample, and the high concentration of Zr-CH_3 groups, also suggests that bipodal species are kinetically or thermodynamically disfavored for this complex. This conclusion is also supported by our unsuccessful attempts to synthesize the dimethoxy version of the precursor, which has also, as of the time of this publication, not been reported in the literature (see SI for details).

Outlook

As evidenced by this last example, distinguishing multiple sites from an ensemble average can be quite challenging, particularly when the molecules are small and thus the differences in the interatomic distances are also limited. This is not a challenge that is unique to NMR-based distance measurements, and it is also seen in analyses of X-ray absorption spectroscopy (XAS) data.[42] There, much like the REDOR example studied here, multisite data are treated as a sum of discrete XAS spectra; inverting this sum is an ill-posed problem. A particularly successful approach has been to use the dynamics of supported clusters to isolate individual contributions to XAS spectra,[42] for instance in variable-temperature studies, or following an exposure to external reactants.[43] Machine learning models are also being used to more directly invert spectral data,[44,45] but again some preliminary structural knowledge is required to aid in the analysis.

Like the XAS examples, NMR distance measurements may contain insufficient information for simultaneous structure and population determinations. If multisite behavior is suspected, it may be preferable to postulate structural models and fit populations alone. In ideal circumstances, obtaining both XAS and NMR data may provide sufficient data to perform this site

and population determination than either method alone struggle to achieve, but this remains to be seen.

We stress that, at least in the case of NMR, the primary challenge is in the differentiation of highly similar structures, such as conformations, or changes in podality. These differences can be far clearer when using methods such as SERS, which has been shown to be highly sensitive to molecular orientation of metal nanoparticle surfaces,[17] and titration methods, which enable the independent measurement of the average podality. When structures differ in their bonding, or when the NMR of the metal center can be done directly, large changes in chemical shifts and quadrupolar coupling do enable the resolution of multiple sites with little difficulty.[11,15,46-52]

Conclusions

Evaluating the homogeneity of surface sites is one of the greatest challenges in the characterization of so-called single-site catalysts. The past few years have shown tremendous progress in the application of NMR-based distance measurement methods for the determination of high-resolution 3D structures for surface sites, but these studies make the flawed assumption that the surface sites are homogeneous. The key question we set out to answer in this study is whether REDOR data is sufficiently information dense to allow for the identification of multiple surface conformers or configurations that are otherwise unresolved in 1D NMR.

We described a Monte Carlo structure search algorithm that compares pairs of conformers to experimental REDOR data and the best-fit single-structure result to assess confidence. The method was benchmarked using synthetic REDOR data produced from various examples found in the literature. We found that the approach could reliably distinguish drastically different conformers when signal-to-noise exceeded 30 but could not distinguish closely related structures. In all but one of the cases studied here, we could not find any evidence of site heterogeneity outside of error. The multi-structure fits agreed with the best-fit single-structure fits, providing some support for the argument that these are indeed single sites. We further cautioned against the use of intermolecular REDOR data to evaluate site heterogeneity.

We lastly applied RESPDOR measurements to gauge the concentration of mono and bipodal zirconocene complexes supported on γ-Al_2O_3 that was thermally activated at different temperatures. While we did notice important changes in the RESPDOR data in agreement with an increase in monopodal species at higher pre-treatment temperatures, we found that all datasets were well fitted to a single configuration, albeit with different surface-to-ligand angles.

In all, we can thus conclude that in ideal circumstances REDOR data can indeed differentiate different surface orientations but cannot differentiate closely related structures. It is advisable to assess the reliability of a given fit using idealized simulations, as was done here, before REDOR data is used to support a claim for site homogeneity or lack thereof.

Author Contributions

FAP performed the solid-state NMR experiments, programming, and data analysis while DBC synthesized the zirconocene functionalized alumina samples. Both authors contributed to the manuscript preparation and project conceptualization.

Conflicts of interest

There are no conflicts to declare.

Acknowledgements

This work was supported by the U.S. Department of Energy (DOE), Office of Basic Energy Sciences (BES), Division of Chemical Sciences, Geosciences, and Biosciences (CSGB), as a part of the Ames National Laboratory catalysis program. Ames National Laboratory is operated for the DOE by Iowa State University under contract no. DE-AC02-07CH11358. Purchase of the 400 MR NMR spectrometer used to obtain results included in this publication was supported by the National Science Foundation under Grant No. CHE 0946687. Any opinions, findings, and conclusions or recommendations expressed in this material are those of the author(s) and do not necessarily reflect the views of the National Science Foundation.

References

1 ~~A. Lesage, M. Lelli, D. Gajan, M.~~ A. Caporini, V. Vitzthum, P. Miéville, J. Alauzun, A. Roussey, C. Thieuleux, A. Mehdi, G. Bodenhausen, C. Copéret, L. Emsley, *J. Am. Chem. Soc.* 2010, **132**, 15459-15461.

2 A. J. Rossini, A. Zagdoun, M. Lelli, A. Lesage, C. Copéret, L. Emsley, *Acc. Chem. Res.* 2013, **46**, 1942-1951.

3 W.-C. Liao, B. Ghaffari, C. P. Gordon, J. Xu, C. Copéret, *Curr. Opin. Colloid. Interface Sci.* 2018, **33**, 63-71.

4 T. Kobayashi, F. A. Perras, I. I. Slowing, A. D. Sadow, M. Pruski, *ACS Catal.* 2015, **5**, 7055-7062.

5 C. Copéret, W.-C. Liao, C. P. Gordon, T.-C. Ong, *J. Am. Chem. Soc.* 2017, **139**, 10588-10596.

6 A. G. M. Rankin, J. Trébosc, F. Pourpoint, J.-P. Amoureux, O. Lafon, *Solid State Nucl. Magn. Reson.* 2019, **101**, 116-143.

7 P. Berruyer, M. Lelli, M. P. Conley, D. L. Silverio, C. M. Widdifield, G. Siddiqi, D. Gajan, A. Lesage, C. Copéret, L. Emsley, *J. Am. Chem. Soc.* 2017, **139**, 849-855.

8 F. A. Perras, J. D. Padmos, R. L. Johnson, L.-L. Wang, T. J. Schwartz, T. Kobayashi, J. H. Horton, J. A. Dumesic, B. H. Shanks, D. D. Johnson, M. Pruski, *J. Am. Chem. Soc.* 2017, **139**, 2702-2709.

9 F. A. Perras, A. L. Paterson, Z. H. Syed, A. J. Kropf, D. M. Kaphan, M. Delferro, M. Pruski, *J. Phys. Chem. C.* 2021, **125**, 13433-13442.

10 F. A. Perras, U. Kanbur, A. L. Paterson, P. Chatterjee, I. I. Slowing, A. D. Sadow, *Inorg. Chem.* 2022, **61**, 1067-1078.

11 R. Jabbour, M. Renom-Carrasco, K. W. Chan, L. Völker, P. Berruyer, Z. Wang, C. M. Widdifield, C. M. Lelli, D. Gajan, C. Copéret, C. Thieuleux, A. Lesage, *J. Am. Chem. Soc.* 2022, **144**, 10270-10281.

12 J. Cunningham, F. A. Perras, *J. Magn. Reson. Open* 2022, **12-13**, 100066.
13 F. A. Perras, A. Arroyave, S. A. Southern, J. V. Lamb, Y. Li, A. LaPointe, M. Delferro, *Chem Commun.* 2023, **59**, 4604-4607.
14 Y. Chen, S. R. Smock, A. H. Flintgruber, F. A. Perras, R. L. Brutchey, A. J. Rossini, 2020, **142**, 6117-6127.
15 Z. Wang, L. A. Völker, T. C. Robinson, N. Kaeffer, G. Menzildjan, R. Jabbour, A. Venkatesh, D. Gajan, A. J. Rossini, C. Copéret, A. Lesage, *J. Am. Chem. Soc.* 2022, **144**, 21530-21543.
16 W. Braun, C. Bösch, L. R. Brown, N. Gō, K. Wütrich, *Biochim. Biophys. Acta.* 1981, **667**, 377-396.
17 R. L. Thimes, A. V. B. Santos, R. Chen, G. Kaur, L. Jensen, D. M. Jenkins, J. P. Camden, *J. Phys. Chem. Lett.* 2023, **14**, 4219-4224.
18 T. Gullion, J. Schaeffer, *J. Magn. Reson.* 1989, **81**, 196-200.
19 K. T. Mueller, T. P. Jarvie, D. J. Aurentz, B. W. Roberts, *Chem. Phys. Lett.* 1995, **242**, 535-542.
20 J.-B. d'Espinose de la Caillerie, C. Fretigny, *J. Magn. Reson.* 1998, **133**, 273-280.
21 H. Schäfer, B. Mädler, F. Volke, *J. Magn. Reson.* 1995, **116**, 145-149.
22 J. D. Gehman, F. Separovic, K. Lu, A. K. Mehta, *J. Phys. Chem. B* 2007, **111**, 7802-7811.
23 G. Jeschke, G.; A. Koch, U. Jonas, A. Godt, *J. Magn. Reson.* 2002, **155**, 72-82.
24 G. Jeschke, *ChemPhysChem* 2002, **3**, 927-932.
25 L. F. Ibáñez, G. Jeschke, *J. Magn. Reson.* 2019, **300**, 28-40.
26 F. Pourpoint, J. Trébosc, R. M. Gauvin, Q. Wang, O. Lafon, F. Deng, J.-P. Amoureux, *ChemPhysChem* 2012, **13**, 3605-3615.
27 A. Zagdoun, G. Casano, O. Ouari, M. Schwarzwälder, A. J. Rossini, F. Aussenac, M. Yulikov, G. Jeschke, C. Copéret, A. Lesage, P. Tordo, L. Emsley, *J. Am. Chem. Soc.* 2013, **135**, 12790-12797.
28 A. Zagdoun, A. J. Rossini, D. Gajan, A. Bourdolle, O. Ouari, M. Rosay, W. E. Maas, P. Tordo, M. Lelli, L. Emsley, A. Lesage, C. Copéret, *Chem Commun.* 2012, **48**, 654-656.
29 T. Kobayashi, F. A. Perras, U. Chaudhary, I. I. Slowing, W. Huang, A. D. Sadow, M. Pruski, *Solid State Nucl. Magn. Reson.* 2017, **87**, 38-44.
30 Z. Gan, *Chem. Commun.* 2006, 4712-4714.
31 Z. H. Syed, D. M. Kaphan, F. A. Perras, M. Pruski, M. S. Ferrandon, E. C. Wegener, G. Celik, J. Wen, C. Liu, F. Dogan, K. I. Goldberg, M. Delferro, *J. Am. Chem. Soc.* 2019, **141**, 6325-6337.
32 A. L. Paterson, D.-J. Liu, U. Kanbur, A. D. Sadow, F. A. Perras, *Inorg. Chem. Frontiers* 2021, **8**, 1416-1431.
33 A. Brinkmann, A. P. M. Kentgens, *J. Am. Chem. Soc.* 2006, **128**, 14758-14759.
34 L. Chen, Q. Wang, B. Hu, O. Lafon, J. Trébosc, F. Deng, J.-P. Amoureux, *Phys, Chem. Chem. Phys.* 2010, **12**, 9395-9405.
35 J. M. Goetz, J. Schaefer, *J. Magn. Reson.* 1997, **127**, 147-154.
36 https://github.com/fperras/INTERFACES
37 R. Wischert, P. Laurent, C. Copéret, F. Delbecq, P. Sautet, *J. Am. Chem. Soc.* 2012, **134**, 14430-14449.
38 C. Morterra, G. Magnacca, *Catal. Today* 1996, **27**, 497-532.
39 R. Wischert, C. Copéret, F. Delbecq, P. Sautet, *Angew. Chem. Int. Ed.* 2011, **50**, 3202-3205.
40 L. T. Zhuravlev, *Langmuir*, 1987, **3**, 316-318.
41 A. R. Siedle, R. A. Newmark, W. M. Lamanna, J. N. Schroepfer, *Polyhedron* 1990, **9**, 301-308.
42 P. K. Routh, N. Marcella, A. I. Frenkel, *J. Phys. Chem. C* 2023, **127**, 5653-5662.
43 K. A. Lomachenko, E. Borfecchia, C. Negri, G. Berlier, C. Lamberti, P. Beato, H. Falsig, S. Bordiga, *J. Am. Chem. Soc.* 2016, **138**, 12025-12028.
44 S. Tetef, N. Govind, G. T. Seidler, *Phys. Chem. Chem. Phys.* 2021, **23**, 23586-23601.
45 J. Timoshenko, A. I. Frenkel, *ACS Catal.* 2019, **9**, 10192-10211.
46 T. Kobayashi, F. A. Perrasm T. W. Goh, T. L. Metz, W. Huang, M. Pruski, *J. Phys. Chem. Lett.* 2016, **7**, 2322-2327.
47 T.-C. Ong, W.-C. Liao, V. Mougel, D. Gajan, A. Lesage, L. Emsley, C. Copéret, *Angew. Chem. Int. Ed.* 2016, **55**, 4743-4747.
48 M. F. Delley, G. Lapadula, F. Núñez-Zarur, A. Comas-Vives, V. Kalendra, G. Jeschke, D. Baabe, M. D. Walter, A. J. Rossini, L. Emsley, O. Maury, C. Copéret, *J. Am. Chem. Soc.* 2017, **139**, 8855-8867.
49 F. A. Perras, A. Venkatesh, M. P. Hanrahan, T. W. Goh, W. Huang, A. J. Rossini, M. Pruski, *J. Magn. Reson.* 2017, **276**, 95-102.
50 J. Camacho-Bunquin, M. Ferrandon, H. Sohn, D. Yang, C. Liu, P. A. Ignacio-de Leon, F. A. Perras, M. Pruski, P. C. Stair, M. Delferro, *J. Am. Chem. Soc.* 2018, **140**, 3940-3951.
51 Z. Wang, S. Patnaik, N. Eedugurala, J. S. Manzano, I. I. Slowing, T. Kobayashi, A. D. Sadow, M. Pruski, *J. Am. Chem. Soc.* 2020, **142**, 2935-2947.
52 D. B. Culver, W. Huynh, H. Tafazolian, M. P. Conley, *Organometallics* 2020, **39**, 1112-1122.